Journal of Volcanology and Geothermal Research 191 (2010) 129–136

Contents lists available at ScienceDirect

Journal of Volcanology and Geothermal Research

journal homepage: www.elsevier.com/locate/jvolgeores

Forecasting eruptions after long repose intervals from accelerating rates of rock fracture: The June 1991 eruption of Mount Pinatubo, Philippines

R. Smith *, C.R.J. Kilburn

AON Benfield UCL Hazard Research Centre, Department of Earth Sciences, University College London, Gower Street, London WC1E 6BT, UK

ARTICLE INFO

Article history:
Received 2 July 2009
Accepted 8 January 2010
Available online 21 January 2010

Keywords:
volcano-tectonic earthquake
eruption forecast
rock fracture
eruption precursor
magma conduit

ABSTRACT

Mount Pinatubo, Philippines erupted on 7th June 1991, after 500 years of repose and two months of detected seismic unrest. Accelerating volcano-tectonic (VT) earthquake rates in the final days before this eruption have previously been used to develop eruption forecasting models based on extension and coalescence of fractures in the volcanic edifice forming a new pathway for magma ascent to the surface. Here, the precursory acceleration in VT earthquake rates is re-analysed with these forecasting models to test their accuracy and sensitivity to how the VT earthquake data are gathered. Binning the data into fixed VT number intervals rather than fixed time intervals gives more precise forecasts, but gives a 'forecast' 24 hours before the eruption began. This is interpreted as the forecast time indicating when the new magma conduit formed. The continued high rate of VT seismicity in the final day before the magma reached the surface is interpreted as widening of the conduit and friction between the magma and country rock during magma ascent.

1. Introduction

Increasing rates of rock fracture, recorded as volcano-tectonic (VT) seismic events, are a common precursor to volcanic eruptions, especially after long repose intervals when there is no existing open conduit (Kilburn, 2003). Models of precursory fracturing rates, developed with the aim of forecasting eruptions at these systems, propose that VT seismic event rates will exhibit a hyperbolic acceleration with a linear decrease in inverse rates in the final one to two weeks before they erupt (Kilburn and Voight, 1998; Kilburn, 2003; Kilburn and Sammonds, 2005). This arises from the growth and coalescence of fractures forming a new pathway between the magma source and the surface (McGuire and Kilburn, 1997; Kilburn, 2003; Kilburn and Sammonds, 2005). Extrapolation of the linear inverse trend to 0, where the rate approaches infinity, gives the expected 'system failure' or eruption time (Voight, 1988; McGuire and Kilburn, 1997; Kilburn and Voight, 1998; Kilburn, 2003; Kilburn and Sammonds, 2005). This trend is likely to give warning times (the time between the recognition of a clear trend and the eruption) of three to five days (Kilburn and Sammonds, 2005). These models also propose that there should be no migration of the 'seismic volume' in this final approach to eruption and that the earthquake locations should be distributed throughout the volume between the magma source and the surface, in the cold country rock. This is consistent with observed hypocentre locations before many eruptions of andesitic to dacitic volcanoes, such as Soufriere Hills, Montserrat in 1995 (Aspinall et al., 1998) and Volcan de Colima, Mexico in 1998 (Zobin et al., 2002). Recent field (Tuffen and Dingwell, 2005; Neuberg et al., 2006) and laboratory (Lavallée et al., 2008; Tuffen et al., 2008) studies indicate that VT earthquakes could also occur within and at the margins of the magma itself, not only in the surrounding colder rocks.

Mount Pinatubo, Philippines, erupted in June 1991 after 500 years of repose and two months of detected unrest, which included earthquake swarms and phreatic activity (Wolfe and Hoblitt, 1996; Newhall et al., 1996). Before these two months, little unrest was noted and there was no scientific monitoring of the volcano (Punongbayan et al., 1996). The eruption began on 7th June with the emergence of a dacite spine. It then evolved into a more explosive eruption, with the first large vertical eruption on 12th June, and the climactic VEI 6 explosion on 15th June (Harlow et al., 1996). Here we analyse precursors to the first emergence of fresh magma on 7th June, when a dacite spine was extruded. It has been proposed that a full connection between the magma reservoir and the surface did not exist until the climactic phase of the eruption (Scandone et al., 2007). However, we believe that the 7th June eruption would have required a fully established fracture connection between the magma reservoir and the surface, though magma within these fractures may have been detached from the magma reservoir in the preclimactic phase of the eruption. We consider that the evolution of the eruption into more explosive phases reflects changes in the magma properties and increased connectivity of the magma body rather than increased connectivity of the fracture network through which the magma ascended. According to these assumptions, it is the initial dacite spine extrusion, not the development into more explosive activity, which

* Corresponding author.
E-mail address: Rosanna.smith@ucl.ac.uk (R. Smith).

0377-0273/$ – see front matter © 2010 Elsevier B.V. All rights reserved.
doi:10.1016/j.jvolgeores.2010.01.006

would have been preceded by accelerating rates of rock fracture as the connection between the reservoir and the surface was established.

Accelerating VT event rates, whose minimum inverse rates had a linear gradient approaching 0 within hours of the time the eruption began, were seen in the final five days before the emergence of the dacite spine (Kilburn, 2003; Kilburn and Sammonds, 2005). Re-analysis of this sequence of VT events for this study indicates that the precision and time of the forecast is highly dependent upon the way that the VT event rate data are grouped. Grouping the data into fixed VT number intervals rather than fixed time intervals gives more precise forecasts, but indicates that the 'failure' occurred 24 hours before the eruption began. This is interpreted as the 'failure' being the formation of a new magma conduit, whilst the additional fracturing that continued in the final day before the magma reached the surface is interpreted as widening of the conduit and friction between the magma and country rock during magma ascent.

1.1. Precursory seismicity at Mount Pinatubo

After unrest was first noted at Pinatubo in late March 1991, new seismometers were installed during April and early May (Harlow et al., 1996; Punongbayan et al., 1996). From 10th May until the first magmatic eruption on 7th June, there were 7 operational telemetered seismometers in the positions shown in Fig. 1 (Lockhart et al., 1996). During this time there were two distinct seismic source regions, shown in Fig. 2; one near the summit of the volcano with depths of 0 to 3 km and one approximately 5 km to the North West with depths of 2 to 6 km. Most of the seismicity in the North West region coincided with phreatic activity in mid to late May. This was followed by a period of relative quiescence from 27th until 31st May. This quiescence coincided with a peak in SO_2 release on 28th May, which was another indicator for the opening of a fracture system on the volcano (Harlow et al., 1996; Scandone et al., 2007). The seismicity in the summit region then accelerated in the days before the eruption on 7th June (Fig. 3). Earthquake locations within the individual swarms did not migrate. Kilburn (2003) found that, in the days before the 7th June 1991 eruption, peaks in the number of VT earthquakes per 4 hours increased such that their inverse was linear and approached zero within hours of the time of the eruption. It was further shown that this trend could have been recognised two to three days before the eruption began (Kilburn and Sammonds, 2005). However, this study used only one grouping for earthquake rates (number per 4 hours) and considered only one possible trend to extrapolate towards the failure point. It would therefore be informative to test how rigorous these results are when the data grouping and method of extrapolating the accelerating seismicity towards the failure point are varied.

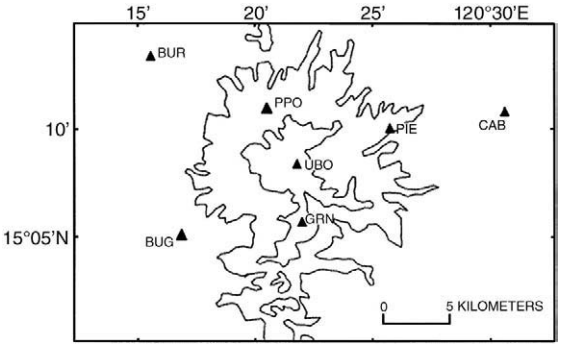

Fig. 1. Positions of telemetered seismometers operating on Pinatubo from 10th May 1991 until the eruption on 7th June 1991. From Harlow et al. (1996).

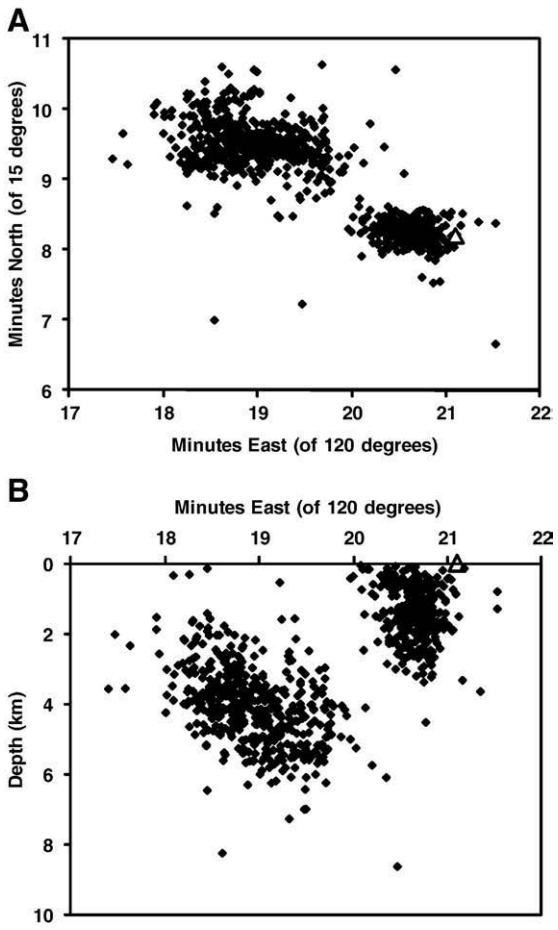

Fig. 2. A). Epicentres and B) depths of earthquakes located on the Pinatubo seismic network from 10th May 1991 until 7th June 1991 (using the catalogue published in Hoblitt et al. (1996)). The open triangle denotes the position of the volcano summit.

The earthquake catalogue used in this study is the catalogue of located earthquakes published in Hoblitt et al. (1996). Before analysing earthquake patterns, catalogues are typically tested for their completeness, and the threshold magnitude adjusted accordingly. Common completeness tests include comparing day and night records, when the background noise levels are expected to differ, and assessing whether the frequency–magnitude distribution deviates from the Gutenburg–

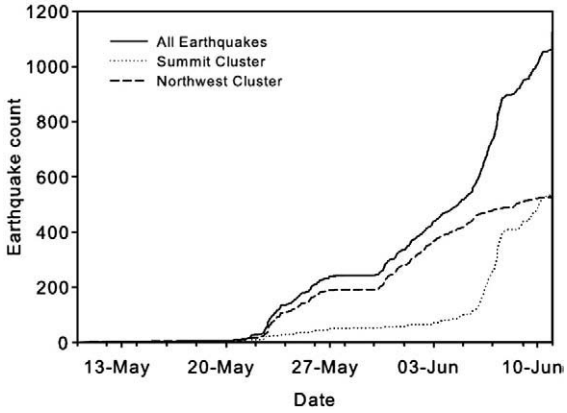

Fig. 3. Cumulative numbers of earthquakes located on the Pinatubo seismic network a) near the volcano summit, b) in the north-west region, and c) in all locations, from 10th May 1991 until 7th June 1991.

Richter relation (Rydelek and Sacks, 1989). This catalogue contains 409 earthquakes in the summit region from 10th May until 7th June 1991 with magnitudes between 0 and 2. They do not exhibit the Gutenburg–Richter frequency–magnitude relation and there are insufficient data to test whether more earthquakes are recorded at different times of day. However, these are the typical data available during volcanic crises at this type of volcano, where the seismic network is often newly installed in response to volcanic unrest and earthquake magnitudes rarely exceed 3 or 4. To discard records on the grounds of completeness would leave no data on which to base forecasts and develop forecasting methods. The data collection was, however, self consistent. That is, during the time considered (mid May to 7th June 1991) the local seismic network used to detect and locate earthquakes was not changed, nor were the detection thresholds. There were also no reported issues with increased noise levels, overlapping events, or damaged seismometers affecting the ability to locate earthquakes until after 7th June (Harlow et al., 1996).

2. Forecasting methods

Rock fracture and material failure models have been used in studies analysing seismicity and ground deformation to forecast eruptions both after a long repose interval (e.g. Cornelius and Voight, 1996; Kilburn and Voight, 1998; Kilburn, 2003), and during extended periods of intermittent lava dome growth (e.g. Voight, 1988; De la Cruz-Reyna and Reyes-Davila, 2001; Smith et al., 2007). Voight's (1988; 1989) failure forecasting method, FFM, is the most widely applied empirical model for forecasting volcanic eruptions from fracturing rates. The rate and acceleration of fracturing, observed through VT seismicity, are related in this empirical law as:

$$\ddot{\Omega} = A\dot{\Omega}^{\alpha} \tag{1}$$

where $\dot{\Omega}$ and $\ddot{\Omega}$ are the rate and acceleration of VT seismicity, and A and α are empirically determined constants with α usually lying between 1 and 2. As $\dot{\Omega}$ approaches infinity, this equation becomes mathematically unstable. Such a condition is associated with a major change in a physical system; in this case with wholesale failure of rock under stress, which creates a pathway for magma ascent. In the limit where $\alpha=1$, there is an exponential increase in seismicity with time and $\dot{\Omega}$ never approaches infinity. In the special case where $\alpha=2$ there is a hyperbolic increase in seismicity with time and $\dot{\Omega}^{-1}$ decreases linearly with time with gradient A. When $\alpha>2$, the inverse trend is convex, when $1<\alpha<2$, the inverse trend is concave, and when $\alpha\leq 1$ the inverse trend never approaches 0.

When the FFM is used to forecast eruptions, the simplest criterion to use is that the eruption is expected when $\dot{\Omega}$ approaches infinity or $\dot{\Omega}^{-1}=0$. The failure time (t_f) is then forecast by integrating Eq. (1) to obtain (Voight, 1989):

$$t_f - t_* = \frac{\dot{\Omega}_*^{1-\alpha}}{A(\alpha-1)} \tag{2}$$

where t_* is an arbitrary time and $\dot{\Omega}_*$ is the seismicity rate at that time. The empirical constants A and α must be determined before using Eq. (2). The only non-iterative way to find these values is to plot the logarithm of $\ddot{\Omega}$ against the logarithm of $\dot{\Omega}$ with the gradient giving α and the intercept giving A (Cornelius and Voight, 1995; Smith et al., 2007). This is based on the logarithmic form of Eq. (1):

$$\log\left(\ddot{\Omega}\right) = \alpha \log\left(\dot{\Omega}\right) + \log(A) \tag{3}$$

The failure time can also be found graphically by extending the inverse trend to the point where $\dot{\Omega}^{-1}=0$, and hence $\dot{\Omega}$ approaches ∞. When the value of α is not known beforehand and data are scarce, it may be difficult to obtain precise forecasts using the FFM (Cornelius and Voight, 1995). Both the graphical method and use of Eq. (2) are simpler in the special and common case of $\alpha=2$, as the inverse trend is linear and Eq. (2) simplifies to Eq. (4)

$$t_f - t_* = \frac{1}{A\dot{\Omega}^*} \tag{4}$$

It has previously been shown that the acceleration in subcritical crack growth under conditions of constant stress can be described by the FFM with $1\leq\alpha\leq 2$; often $\alpha=2$ in the final approach to failure (Cornelius and Scott, 1993; McGuire and Kilburn, 1997). It has further been proposed that the acceleration in cracking events will be exponential ($\alpha=1$) when precursory fracturing begins and is dominated by the formation and reactivation of new fractures (McGuire and Kilburn, 1997). It is then expected to become hyperbolic ($\alpha=2$) when the fracturing becomes dominated by the growth and coalescence of already active fractures in the final days before an eruption (McGuire and Kilburn, 1997; Kilburn and Voight, 1998; Kilburn, 2003; Kilburn and Sammonds, 2005).

In volcanic systems, seismic event rates are typically the most readily available measure of VT seismicity. If it is assumed that the average fracture length extension per seismic event is constant, then the FFM can be applied with $\dot{\Omega}$ representing the seismic event rate. If it is also assumed that the bulk strain and seismic event rate are dominated by fracture growth rather than activation of new fractures, then Kilburn's (2003) deterministic approach shows that α is 2 and the linear inverse trend has a gradient γ defined as:

$$\gamma = \pi\left(S^2 / Y'\right) w\Delta c^2 / nRT \tag{5}$$

where S is the remotely applied differential stress, Y' is the effective Young's modulus of the edifice rocks, w is the width of an extending crack, Δc is the crack extension per seismic event, n is the number of moles of rock in the cracking process zone, T is the temperature in Kelvin, and R is the ideal gas constant. Kilburn (2003) later showed, using a model based on the Griffith energy balance and a Boltzmann distribution of random energy fluctuations, that the peaks in seismic event rate rather than all event rate values should reveal the linear inverse trend. These peaks are believed to represent a larger scale of cracking than the individual events, with the interaction between these two scales of cracking giving the expected gradient of this linear inverse minima trend (Kilburn, 2003) from division of the overall inverse rate gradient by $\Delta c_1/\delta_1$ (larger scale fracture extension/adjacent thickness of rock over which strain energy is released):

$$\gamma = \pi\left(S^2 / Y'\right) W_m / \rho RT \tag{6}$$

where W_m and ρ are the rock's molar mass and mean density. This adaptation for inverse rate minima rather than all inverse rates eliminates all scale dependent variables, leaving γ^* as a function of scale independent physical parameters. For volcanic edifice conditions, $\gamma^* = (4.5\pm 3.2)\times 10^{-3}$. Gradients were found to lie within this expected range for seismic event rates before eruptions at Montserrat, West Indies, and Pinatubo, Philippines (Kilburn, 2003) and acoustic emissions during high temperature laboratory deformation of andesite (Smith et al., 2009). Kilburn's (2003) multiscale fracture model is thus a deterministic method to forecast when fractures will coalesce to form a new conduit, allowing a new eruption to begin, whereas the FFM is purely empirical.

In this study, three similar methods are used to generate forecasts, (1) the FFM in the form of Eq. (2) with α and A determined using the logarithmic form of the FFM (Eq. (3)) as in Smith et al. (2007), (2) extrapolation of the linear trend in inverse rates to zero, i.e. the FFM with $\alpha=2$ assumed, and (3) extrapolation of the linear trend in minima in inverse rates to zero, i.e. Kilburn's (2003) multiscale fracture model, hereafter referred to as MFM. Comparisons are also made between two

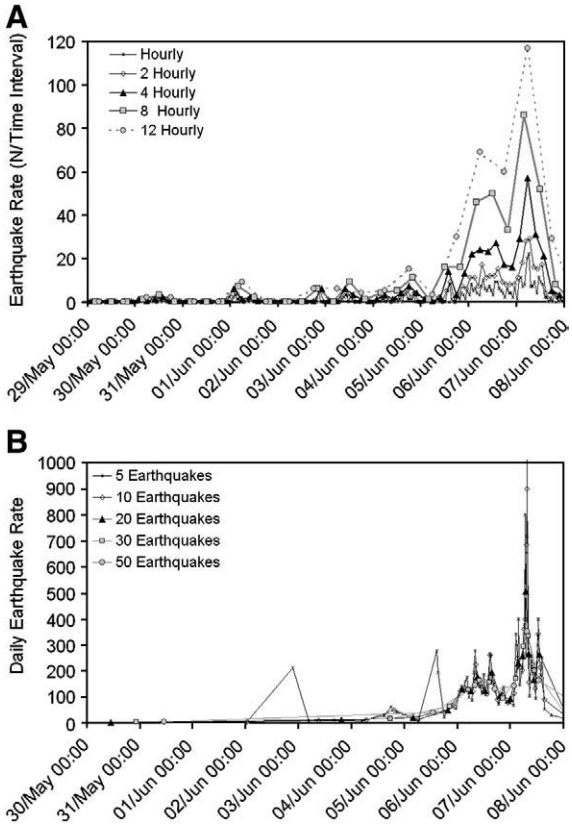

Fig. 4. Rates of time- and number-binned earthquakes located in the summit region of Mount Pinatubo from 27th May until 7th June. Time-binned rates (A) are shown for one, two, four, eight and twelve hour intervals. Number-binned rates (B), scaled to daily rates, are shown for 5, 10, 20, 30, and 50 earthquake intervals.

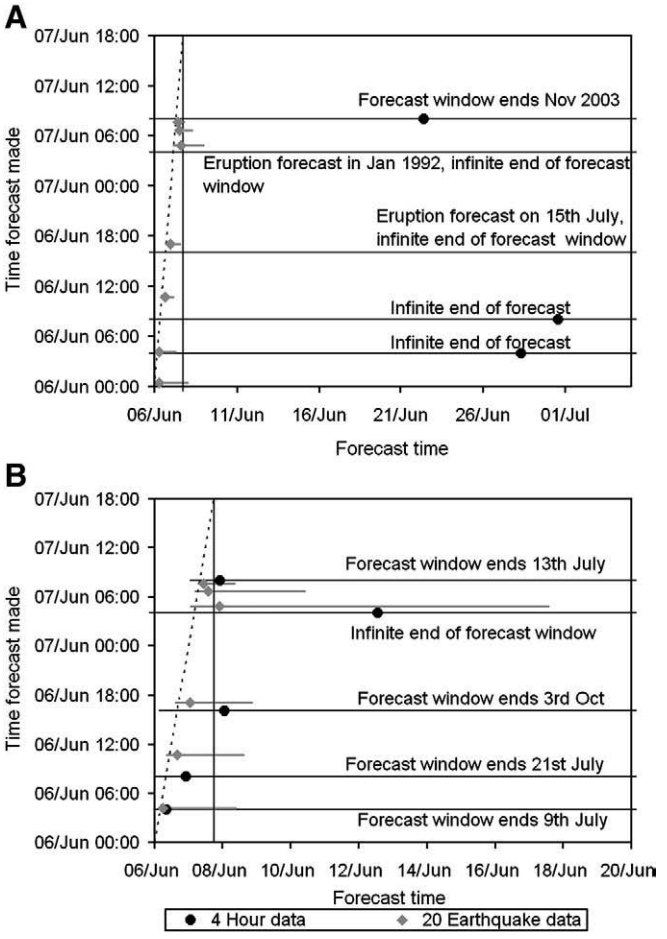

Fig. 5. Forecasts of the 7th June 1991 eruption of Mount Pinatubo using the failure forecasting method (FFM) with earthquakes located in the summit region from A) 27th May, and B) 3rd June. Forecasts were generated from T-binned data (black circles) and N-binned data (grey diamonds). As time progresses up the *y* axis, all data up to that time are used to generate a forecast using the FFM. The y coordinate of each forecast is the time it is made, and the *x* coordinate is the expected eruption time, with the *x* error bars showing the extent of the forecast window. The black vertical line shows the time the eruption occurred and the dashed line shows where the actual time and forecast time are equal, with only points to the right of this line constituting a forecast.

different start dates for the data analysis to see how this influences forecast precision and accuracy: 27th May, which is after the swarm of activity to the North-West of the volcano had ceased and a few days before the clear acceleration began, and 3rd June, the date used in Kilburn (2003), which is when the clear acceleration began. Earthquake data are analysed for the summit region only, using the record from Hoblitt et al. (1996), because only earthquakes in this region accelerated before the eruption (Fig. 3). There were 350 recorded earthquakes in this region from 27th May until the eruption began.

Earthquake rates can be calculated for fixed time intervals (where $\dot{\Omega}$ = number of earthquakes during time interval/length of time interval) or for fixed number intervals (where $\dot{\Omega} = N$/time per N earthquakes), referred to hereafter as T-binned and N-binned data respectively. N-binned data give equal weight to all events, whilst the T-binned data give equal weight to each time interval. This results in the N-binned data giving more weight to the latter part of the accelerating trend than the T-binned data. Forecasts from these two measures of earthquake rate are compared. Earthquake rates were plotted for a range of time and number intervals in order to identify which intervals would be best for this study (Fig. 4). Time bins of 4 hours and number bins of 20 earthquakes were chosen, as these give the best balance between increasing amount of rate data with shorter time and number bins and loss of signal in the noise when bins are too short (Smith et al., 2007).

3. Results

3.1. Method 1: The FFM with variable α

Forecasts calculated using Eq. (2), with A and α calculated using the log–log method described above, are shown in Fig. 5 for both data bin types and both start dates. The position on the *y* axis represents the time when the forecast is made, with only data before this point used to generate the forecast. The position on the *x* axis represents the time the eruption is forecast to begin. The forecast window lengths were found by combining the standard errors (one standard deviation) of each of the parameters. Parameters A and α and their errors for each forecast calculation are shown in Table 1. There were insufficient data to generate any forecasts from the summit data until the early hours of 6th June (~40 hours before the eruption), as 3 $\dot{\Omega}$ values that are larger than the last maximum are needed to calculate the first A and α values to generate the first forecast. It was found that errors in α resulted in extremely long forecast windows for the T-binned data (with both start dates). The forecast window was always at least a month long for the data beginning on 3rd June (Fig. 5B, black symbols), and infinite except for one forecast window over 20 years long for the data beginning on 27th May (Fig. 5A, black symbols). For the N-binned data (Fig. 5, grey symbols), the forecast windows were far shorter due to the α values having smaller error bounds, but forecast windows generated on the 6th June from data beginning on 27th May ended before the eruption began. On 7th June, α errors were larger, resulting in longer forecast windows that included the time of the eruption. Forecast windows from the N-binned data were generally longer for the data starting on 3rd June, probably due to there being fewer data to constrain the trend.

Table 1
A and α values and their errors calculated from log–log plots for each forecast calculation in Fig. 5.

Data set used	No. of $\ddot{\Omega}$ values used	α value	*A* value	
Earthquakes grouped per 4 hours from 3rd June	3	3.3 ± 1.3	0.30 + 6.4/−0.28	$\times 10^{-3}$
	4	2.4 ± 0.95	1.9 + 20.8/−1.7	
	5	1.9 ± 0.79	5.3 + 40.4/−4.7	
	6	1.4 ± 0.80	17 + 153/−15.6	
	7	2.1 ± 0.74	3.1 + 25.4/−2.8	
Earthquakes grouped per 4 hours from 27th May	3	0.93 ± 0.75	13.5 + 30.5/−9.4	$\times 10^{-3}$
	4	1.3 ± 0.47	9.2 + 14.3/−5.6	
	5	1.3 ± 0.32	9.5 + 10.3/−4.9	
	6	1.2 ± 0.27	10.5 + 9.6/−5.0	
	7	1.0 ± 0.28	12.9 + 13.9/−6.7	
	8	1.4 ± 0.36	7.7 + 13.0/−4.8	
Earthquakes in groups of 20 from 3rd June	3	2.1 ± 0.02	0.056 + 0.0038/−0.0035	
	4	1.6 ± 0.29	0.22 + 0.51/−0.15	
	5	1.5 ± 0.23	0.33 + 0.56/−0.21	
	6	1.3 ± 0.25	0.63 + 1.29/−0.42	
	7	1.5 ± 0.27	0.33 + 0.84/−0.24	
	8	1.7 ± 0.27	0.15 + 0.41/−0.11	
Earthquakes in groups of 20 from 27th May	3	1.9 ± 0.08	0.089 + 0.023/−0.018	
	4	2.0 ± 0.04	0.079 + 0.012/−0.011	
	5	1.7 ± 0.17	0.15 + 0.12/−0.072	
	6	1.6 ± 0.15	0.20 + 0.16/−0.089	
	7	1.5 ± 0.17	0.29 + 0.31/−0.15	
	8	1.6 ± 0.18	0.21 + 0.26/−0.12	
	9	1.7 ± 0.18	0.14 + 0.18/−0.081	

3.2. Method 2: The FFM linear inverse rate mean trend

When α is fixed at 2, forecasts are generated by extrapolation of the linear inverse trend to the time axis, as described in the forecasting section. Forecasts generated using this method for both start dates and both data bin types are shown in Fig. 6. All forecast windows were far shorter than those for the FFM with variable α. For the T-binned data, the data start date of 3rd June gives far shorter forecast windows than the data start date of 27th May. All forecast windows generated using T-binned data from the 27th May (Fig. 6A, black symbols) started when the forecast was made and were at least 5 days long, until the forecast made using data until 8 am on 7th June, which gave a forecast window 4 1/2 days long. Using T-binned data from the 3rd June (Fig. 6B, black symbols), forecasts generated on the 6th June extended from the time the forecast was made until 8th or 9th June. Once again, forecast windows generated from the N-binned data (Fig. 6, grey symbols) were shorter than those generated from the number of earthquakes per 4 hours and often *forecast* that the eruption had already begun.

3.3. Method 3: The MFM (i.e. linear trend in inverse rate minima)

Fig. 7 shows the forecasts generated from the four groupings of summit data using the multiscale fracture model (Kilburn, 2003), where the forecast of the eruption time is the linear extrapolation of minima in inverse rates to the time axis. For the T-binned data, forecast windows were considerably shorter than they were using the other methods. All forecasts generated after midday on 6th June from the data beginning on 27th June (Fig. 7A, black symbols) gave forecast windows from a few hours after the forecast was made until the morning of 9th June. Using the T-binned data beginning on the 3rd June (Fig. 7B, black symbols), forecasts generated after midday on 6th June gave forecast windows from the time the forecast was made until the afternoon of 8th June. For the N-binned data beginning on 27th May (Fig. 7A, grey symbols) forecast windows were similar lengths to those from the T-binned data, but they were shorter for the data beginning on 3rd June (Fig. 7B, grey symbols). The N-binned data again mostly forecast that the eruption began early on 6th June, even when using data from after this time.

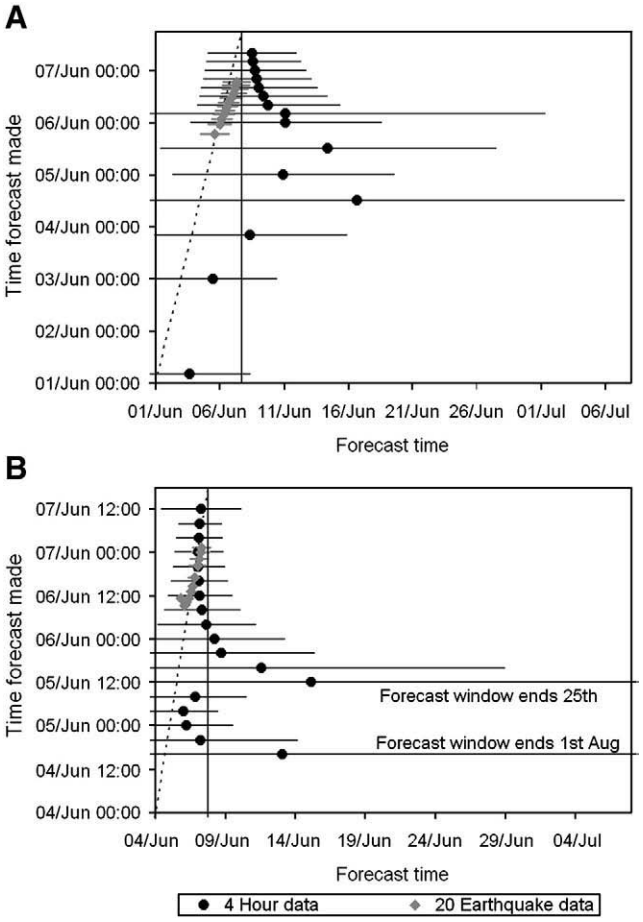

Fig. 6. Forecasts of the 7th June 1991 eruption of Mount Pinatubo using the linear inverse trend form of the failure forecasting method with rates of earthquakes located in the summit region from A) 27th May, and B) 3rd June. Forecast representation, from both T-binned (black symbols) and N-binned (grey symbols) data, is as Fig. 5.

The forecasts from the N-binned data were almost identical for the FFM with $\alpha = 2$ and the MFM, whilst the forecasts from the T-binned data were not. This is because the N-binned data were not as scattered, resulting in a greater proportion of the inverse rate values being considered as minima (Fig. 4). In fact all points from 27th May until 6th June 04:08 were considered as minima, resulting in identical forecasts from these two methods until this point, for both starting dates. The differences after this point are negligible.

4. Discussion

4.1. Comparison of forecasts

The FFM with variable α gave the latest forecast dates with longest forecast windows of the three forecasting methods tested. When α was fixed at two for the FFM, the forecast windows became shorter and earlier. They were shorter and earlier again using the MFM. The FFM parameters *A* and α had larger errors, indicating a poorer fit to the FFM equation, for the T-binned data compared with the N-binned data. This led to longer forecast windows for the T-binned data. The forecast windows were also longer for the T-binned data than the N-binned data for the forecasts from the FFM with α fixed at 2 and for the MFM, although the forecast windows often ended too early. The longer and later forecast windows for T-binned data may be due to the greater weighting given to events in the earlier part of the sequence masking how sharp the acceleration is. N-binned data until the morning of 6th June or

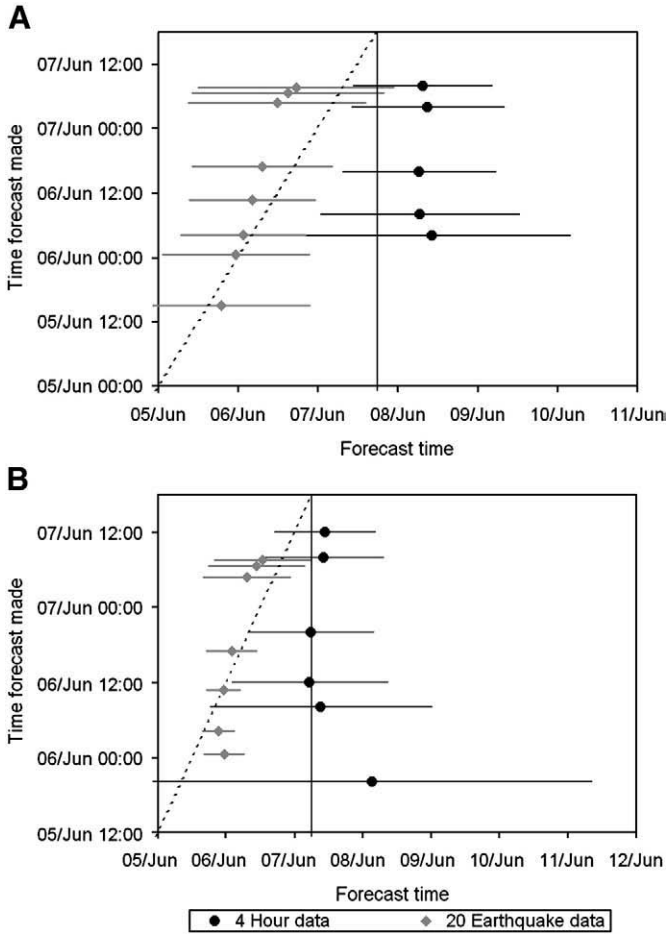

Fig. 7. Forecasts of the 7th June 1991 eruption of Mount Pinatubo using the multiscale fracture model with rates earthquakes located in the summit region from A) 27th May, and B) 3rd June. Forecast representation, from both T-binned (black symbols) and N-binned (grey symbols) data, is as Fig. 5.

later analysed using the FFM consistently gave an eruption forecast within a few hours of the time the forecast was made (Figs 5 and 6). The forecast was consistently on the morning of 6th June for N-binned data analysed with the MFM, compared to an actual eruption time of 7th June in the afternoon. This may arise due to the event rates accelerating until the morning of 6th June, and then remaining at a similar level until a final spike in event rate coincident with the onset of the eruption on 7th June (Fig. 4).

Use of event rate data starting on the earlier date of 27th May gave longer forecast windows and less accurate preferred forecast dates compared with the trends obtained starting on 3rd June for the T-binned data for all three forecasting methods. In contrast, the influence of the earlier start date on forecasts from N-binned data was negligible or slightly improved forecast precision in all cases. This demonstrates that forecasts from T-binned data can be distorted or masked by inclusion of data from before a clear acceleration emerges, whereas forecasts from N-binned data are not affected in this way. Although the forecasts from N-binned data were consistently too early, they were more robust and precise than those from T-binned data.

4.2. Precursory fracturing regime

Some models of precursory fracturing include an evolution from exponential to hyperbolic acceleration fracturing rates as the fracturing regime changes from the formation and reactivation of new fractures to the extension and coalescence of already active fractures (McGuire and Kilburn, 1997; Kilburn and Voight, 1998; Kilburn, 2003; Kilburn and Sammonds, 2005). Using the FFM, this is a change in the exponent α from 1 to 2. If the sequence from 27th May includes this change of regime, it is expected that: 1) the FFM exponent will be lower for the earlier start date (27th May rather than 3rd June); 2) the exponent will become gradually higher as event rate data from later dates are included to update the forecasts; and 3) the exponent will be lower for the T-binned data due to the greater weighting given to events earlier in the sequence for this type of data binning. The earlier start date effect was seen in the T-binned data, but not the N-binned data (Table 1). Inclusion of later data to update the forecasts did not affect the exponent value for either start date or type of data binning (Table 1). The expected higher exponent for N-binned data was seen for the earlier start date only. The lower exponent values, seen only for the T-binned data with the earlier start date, could be explained by too much weighting given to data before there was any acceleration rather than a change in α from one to two as the fracturing regime changed. There is thus no evidence of an evolution from exponential to hyperbolic acceleration in fracturing rates.

When using the multiscale fracture model, it is expected that the gradient of minima in inverse rates will be limited to $(4.5 \pm 3.2) \times 10^{-3}$ by the scale independent critical bulk strain (Kilburn, 2003). The T-binned data always gave gradients within this range, but the gradients for the N-binned data were all greater than this range at $(3.9 \pm 1.5) \times 10^{-2}$ (Table 2). This can also be seen on Fig. 8, where the inverse minima for the N-binned data have a far steeper gradient than the minima in T-binned data. The scale dependent variables in the critical bulk strain were eliminated in the argument for using peak rates rather than all rates to generate a forecast (Kilburn, 2003). If they are not eliminated in this way, the scale independent critical bulk strain must be multiplied by $\Delta c_1/\delta_1$, where Δc_1 is the crack extension at peak event rates and δ_1 is the thickness of rock across which strain energy is released for the larger scale cracks. The result that the inverse gradient is 5 to 10 times larger when the peak rate scaling cannot be used indicates that $\Delta c_1/\delta_1$ is between 5 and 10.

Table 2
Gradients of the linear trend in inverse rate minima used to calculate the forecasts shown in Fig. 7.

Data used	Date and time forecast made	No. of data pts used	Gradient
Number of earthquakes located in the summit region per 4 hours from 27th May 1991	6th June, 04:00	3	-0.0038 ± 0.0004
	6th June, 08:00	4	-0.0039 ± 0.0003
	6thJune, 16:00	5	-0.0039 ± 0.0002
	7th June, 04:00	6	-0.0039 ± 0.0002
	7th June, 08:00	7	-0.0039 ± 0.0002
Number of earthquakes ocated in the summit region per4 hours from 3rd June 1991	5th June, 20:00	3	-0.0053 ± 0.0029
	6th June, 08:00	4	-0.0063 ± 0.0019
	6th June, 12:00	5	-0.0066 ± 0.0014
	6th June, 20:00	6	-0.0066 ± 0.0011
	7th June, 08:00	7	-0.0062 ± 0.0009
	7th June, 12:00	8	-0.0062 ± 0.0008
Time per 20 earthquakes located in the summit region from 27th May 1991	5th June, 15:02	3	-0.054 ± 0.005
	5th June, 00:27	4	-0.052 ± 0.004
	6th June, 04:08	5	-0.051 ± 0.003
	6th June, 10:43	6	-0.050 ± 0.003
	6th June, 17:00	7	-0.048 ± 0.003
	7th June, 04:50	8	-0.046 ± 0.004
	7th June, 06:41	9	-0.045 ± 0.004
	7th June, 07:38	10	-0.043 ± 0.004
Time per 20 earthquakes located in the summit region from 3rd June 1991	6th June, 00:27	3	-0.033 ± 0.002
	6th June, 04:08	4	-0.034 ± 0.002
	6th June, 10:43	5	-0.033 ± 0.002
	6th June, 17:00	6	-0.031 ± 0.002
	7th June, 04:50	7	-0.027 ± 0.004
	7th June, 06:41	8	-0.025 ± 0.003
	7th June, 07:38	9	-0.024 ± 0.003

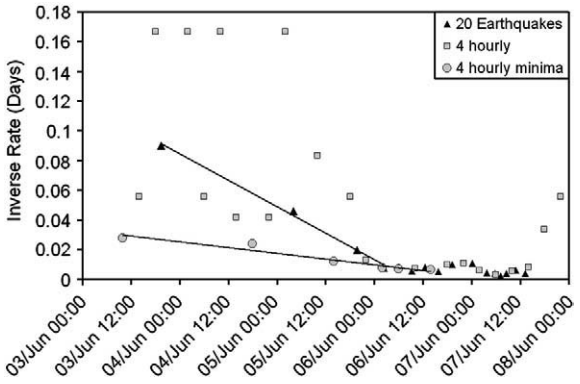

Fig. 8. Inverse earthquake rates between 3rd and 7th June 1991 at Mount Pinatubo calculated at four hourly intervals (grey symbols) and 20 earthquake intervals (black symbols). Note that the linear fit to the minima in 4 hourly inverse rates (grey circles) is much shallower than the fit to the 20 earthquake inverse rates (black triangles).

The forecasts from the N-binned data from all three forecasting methods indicate that fracturing rates were accelerating towards a potential failure on the 6th of June. Rates then stabilised, before a final acceleration on 7th June, when the eruption began. The preferred forecast date of 6th June may indicate that the new conduit had formed by that day, with an additional day taken for the magma to migrate towards the surface. During that day, the event rates were approximately constant until they increased as the magma emerged at the surface (Fig. 4). Stick–slip earthquakes arising from friction between the magma body and the conduit, in addition to fracturing of the surrounding rocks as the conduit widened to accommodate the ascending magma, could have caused the additional earthquakes after the conduit was formed. It has been shown that these earthquakes at the conduit margins may be seismogenic (Neuberg et al., 2006; Tuffen et al., 2008). This model of precursory fracturing at Mount Pinatubo in 1991 is shown schematically in Fig. 9. Stick–slip earthquakes typically occur in bursts, but when the shear strain rate and the normal stress acting on the sliding fracture surface are constant and the rate is considered over a timescale long enough to smooth out these bursts,

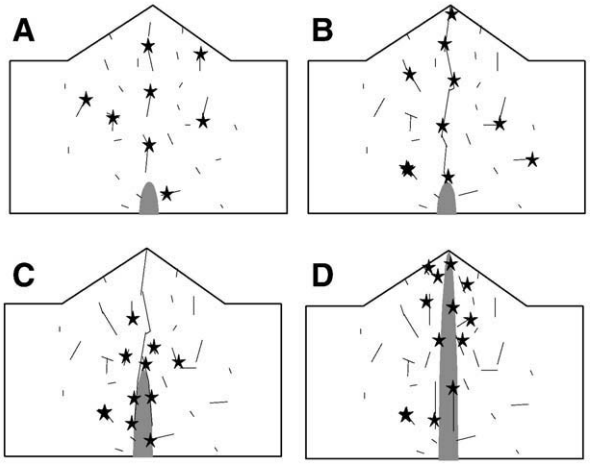

Fig. 9. Schematic diagram of expected fracturing patterns prior to the 7th June 1991 eruption of Mount Pinatubo. Black lines show fractures, with stars representing VT earthquake locations and grey representing the magma body. Initially, A) fractures within the volume between the magma body and the surface extend and coalesce at an accelerating rate described by the multiscale fracture model (Kilburn, 2003), until B) fractures connect the magma body to the surface. When the magma begins to ascend, C) the fracture connecting the magma to the surface is forced to widen deforming the surrounding rock causing further earthquakes in addition to those due to friction between the magma and the conduit walls. This continues until D) the magma reaches the surface. Note that the seismically active volume does not migrate during the progression from A) to D).

the rate of stick–slip events is constant (Sammonds and Ohnaka, 1998). Therefore, if the pressure driving the ascent of the magma and the normal force acting on the surface between the ascending magma and the country rock are near constant, there will be a near constant rate of stick–slip earthquakes at the magma conduit margins and near constant deformation and cracking of the surrounding rocks as the conduit widens. This could explain the nearly constant earthquake rate in the final 24 hours before a final spike in event rates at the time of the eruption.

5. Conclusions

Forecasts of the 7th June 1991 eruption of Mount Pinatubo from earthquake rates were compared between number- and time-binned data, three forecasting methods, and two different start dates for the analysis. The FFM with variable α gave longer forecast windows than the FFM with α fixed at two or the MFM. Forecast windows (for all methods) were longer for time-binned data than number-binned data. However, number-binned earthquake data consistently gave forecast windows that ended before the eruption began. For time-binned earthquake data, the multiscale fracture model (Kilburn, 2003) gave the most accurate forecasts, but the accuracy was sensitive to the start date for data analysis. The number-binned data showed less sensitivity to the start date for data analysis and showed a better fit to all forecasting models. Number-binned data therefore give more robust forecasts than time-binned data. However, the forecasts from this data grouping were consistently a day before the eruption began. This is interpreted as a valid forecast for the time that the conduit formed, with the conduit widening and the magma migrating towards the surface in the final day between conduit formation and the eruption onset.

Acknowledgements

Peter Sammonds is thanked for discussions on fracture propagation in volcanic systems. RS was funded by a NERC PhD studentship and a NERC research grant. Two anonymous reviewers are thanked for helpful comments, which improved the quality of this paper.

References

Aspinall, W.P., Miller, A.D., Lynch, L.L., Latchman, J.L., Stewart, R.C., White, R.A., Power, J.A., 1998. Soufriere Hills eruption, Montserrat, 1995–1997: volcanic earthquake locations and fault plane solutions. Geophysical Research Letters 25, 3397–3400.

Cornelius, R. R., Voight, B., 1996. Real-time seismic amplitude measurement (RSAM) and seismic spectral amplitude measurement (SSAM) analyses with the Materials Failure Forecast Method (FFM), June 1991 explosive eruption at Mount Pinatubo. In: Punongbayan, R.S., Newhall, C.G. (Eds.), Fire and mud: eruptions and lahars of Mount Pinatubo, Philippines. University of Washington Press, Seattle; PHIVOLCS, Quezon City, pp. 249–267.

Cornelius, R.R., Scott, P.A., 1993. A materials failure relation of accelerating creep as empirical description of damage accumulation. Rock Mechanics and Rock Engineering 26 (3), 233–252.

Cornelius, R.R., Voight, B., 1995. Graphical and PC-software analysis of volcano eruption precursors according to the Materials Failure Forecast Method (FFM). Journal of Volcanology and Geothermal Research 64 (3–4), 295–320.

De la Cruz-Reyna, S., Reyes-Davila, G.A., 2001. A model to describe material-failure phenomena: applications to short-term forecasting at Colima volcano, Mexico. Bulletin of Volcanology 63, 297–308.

Harlow, D. H., Power, J.A., Laguerta, E.P., Ambubuyog, G., Hoblitt, R.P., 1996. Precursory seismicity and forecasting of the June 15, 1991, eruption of Mount Pinatubo. In: Punongbayan, R.S., Newhall, C.G. (Eds.), Fire and mud: eruptions and lahars of Mount Pinatubo, Philippines. University of Washington Press, Seattle; PHIVOLCS, Quezon City, pp. 233–247.

Hoblitt, R.P., Mori, J., Power, J.A., 1996. Computer visualization of earthquake hypocenters. In: Punongbayan, R.S., Newhall, C.G. (Eds.), Fire and mud: eruptions and lahars of Mount Pinatubo, Philippines. University of Washington Press, Seattle; PHIVOLCS, Quezon City, pp. 383–385.

Kilburn, C.R.J., 2003. Multiscale fracturing as a key to forecasting volcanic eruptions. Journal of Volcanology and Geothermal Research 125, 271–289.

Kilburn, C.R.J., Sammonds, P.R., 2005. Maximum warning times for imminent volcanic eruptions. Geophysical Research Letters 32 (24) article number L24313.

Kilburn, C.R.J., Voight, B., 1998. Slow rock fracture as eruption precursor at Soufriere Hills Volcano, Montserrat. Geophysical Research Letters 25 (19), 3665–3668.

Lavallée, Y., Meredith, P.G., Dingwell, D.B., Hess, K.U., Wassermann, J., Cordonnier, B., Gerik, A., Kruhl, J.H., 2008. Seismogenic lavas and explosive eruption forecasting. Nature 453, 507–510.

Lockhart, A. B., Marcial, S., Ambubuyog, G., Laguerta, E.P., Power, J.A., 1996. The first Mount Pinatubo telemetered seismic network. In: Punongbayan, R.S., Newhall, C.G. (Eds.), Fire and mud: eruptions and lahars of Mount Pinatubo, Philippines. University of Washington Press, Seattle; PHIVOLCS, Quezon City, pp. 215–223.

McGuire, W., Kilburn, C.R.J., 1997. Forecasting volcanic events: some contemporary issues. Geologische Rundschau 86, 439–445.

Neuberg, J., Tuffen, H., Collier, L., Green, D., Powell, T., Dingwell, D.B., 2006. The trigger mechanism of low-frequency earthquakes on Montserrat. Journal of Volcanology and Geothermal Research 153, 37–50.

Newhall, C.G., Daag, A.S., Delfin, F.G., Hoblitt, R.P., McGeehin, J., Pallister, J.S., Regalado, M.T.M., Rubin, A.M., Tamayo, R.A., Tubianosa, B., Umbal, J.V., 1996. Eruptive history of Mount Pinatubo. In: Punongbayan, R.S., Newhall, C.G. (Eds.), Fire and mud: eruptions and lahars of Mount Pinatubo, Philippines. University of Washington Press, Seattle; PHIVOLCS, Quezon City, pp. 165–195.

Punongbayan, R.S., Newhall, C.G., Bautista, M.L.P., Garcia, D., Harlow, D.H., Hoblitt, R.P., Sabit, J.P., Solidum, R.U., 1996. Eruption hazard assessments and warnings. In: Punongbayan, R.S., Newhall, C.G. (Eds.), Fire and mud: eruptions and lahars of Mount Pinatubo, Philippines. University of Washington Press, Seattle; PHIVOLCS, Quezon City, pp. 67–85.

Rydelek, P.A., Sacks, I.S., 1989. Testing the completeness of earthquake catalogues and the hypothesis of self-similarity. Nature 337, 251–253.

Sammonds, P.R., Ohnaka, M., 1998. Evolution of microseismicity during frictional sliding. Geophysical Research Letters 25, 699–702.

Scandone, R., Cashman, K.V., Malone, S.D., 2007. Magma supply, magma ascent and the style of volcanic eruptions. Earth and Planetary Science Letters 253, 513–529.

Smith, R., Kilburn, C.R.J., Sammonds, P.R., 2007. Rock fracture as a precursor to lava dome eruptions at Mount St Helens from June 1980 to October 1986. Bulletin of Volcanology 69, 681–693.

Smith, R., Sammonds, P.R., Kilburn, C.R.J., 2009. Fracturing of volcanic systems: experimental insights into pre-eruptive conditions. Earth and Planetary Science Letters 280, 211–219.

Tuffen, H., Dingwell, D.B., 2005. Fault textures in volcanic conduits: evidence for seismic trigger mechanisms during silicic eruptions. Bulletin of Volcanology 67, 370–387.

Tuffen, H., Smith, R., Sammonds, P.R., 2008. Evidence for seismogenic fracture of silicic magma. Nature 453, 511–514.

Voight, B., 1988. A method for prediction of volcanic eruptions. Nature 332, 125–130.

Voight, B., 1989. A relation to describe rate-dependent material failure. Science 243, 200–203.

Wolfe, E.W., Hoblitt, R.P., 1996. Overview of the eruptions. In: Punongbayan, R.S., Newhall, C.G. (Eds.), Fire and mud: eruptions and lahars of Mount Pinatubo, Philippines. University of Washington Press, Seattle; PHIVOLCS, Quezon City, pp. 3–20.

Zobin, V.M., Amezcua, M.G., Davila, G.A.R., Dominguez, T., Chacon, J.C.C., Alvarez, J.M.C., 2002. Comparative characteristics of the 1997–1998 seismic swarms preceding the November 1998 eruption of Volcan de Colima, Mexico. Journal of Volcanology and Geothermal Research 117, 47–60.